# Interaction of Horse Heart and *Thermus thermophilus* Type *c* Cytochromes with Phospholipid Vesicles and Hydrophobic Surfaces

Sophie Bernad,* Silke Oellerich,† Tewfik Soulimane,‡ Sylvie Noinville,* Marie-Hélène Baron,* Maité Paternostre,§ and Sophie Lecomte*

*Laboratoire de Dynamique, Interactions et Réactivité, CNRS-Université Paris VI, Thais, France; †Max-Planck Institut für Strahlenchemie, Mülheim, Germany; ‡Paul Scherrer Institut, Life Sciences, Structural Biology, OSRA/008, Villigen, Switzerland; and §URA 2096, CEA-CNRS, DBJC/SBFM CEA-Saclay, Gif/Yvette, France

ABSTRACT The binding of horse heart cytochrome *c* (cyt-*c*) and *Thermus thermophilus* cytochrome $c_{552}$ (cyt-$c_{552}$) to dioleoyl phosphatidylglycerol (DOPG) vesicles was investigated using Fourier transform infrared (FTIR) spectroscopy and turbidity measurements. FTIR spectra revealed that the tertiary structures of both cytochromes became more open when bound to DOPG vesicles, but this was more pronounced for cyt-*c.* Their secondary structures were unchanged. Turbidity measurements showed important differences in their behavior bound to the negatively charged DOPG vesicles. Both cytochromes caused the liposomes to aggregate and flocculate, but the ways they did so differed. For cyt-*c,* more than a monolayer was adsorbed onto the liposome surface prior to aggregation due to charge neutralization, whereas cyt $c_{552}$ caused aggregation at a protein/lipid ratio well below that required for charge neutralization. Therefore, although cyt-*c* may cause liposomes to aggregate by electrostatic interaction, cyt-$c_{552}$ does not act in this way. FTIR-attenuated total reflection spectroscopy (FTIR-ATR) revealed that cyt-*c* lost much of its secondary structure when bound to the hydrophobic surface of octadecyltrichlorosilane, whereas cyt-$c_{552}$ folds its domains into a $\beta$-structure. This hydrophobic effect may be the key to the difference between the behaviors of the two cytochromes when bound to DOPG vesicles.

## INTRODUCTION

*c*-Type cytochromes act as electron carriers between cytochrome *c* reductase and cytochrome *c* oxidase in the respiratory chain of aerobic cells. Horse heart cytochrome *c* (cyt-*c*) is a soluble protein with a positively charged lysine-rich region around the exposed heme edge that constitutes the binding domain based on electrostatic interactions with both reaction partners. Although the topology of the mitochondrial membrane is not known, it is very likely that cyt-*c* remains in the electrical double layer of the membrane for the transfer of electrons from cytochrome *c* reductase to cytochrome *c* oxidase. This obvious importance of membrane interactions for the function of *c*-type cytochromes has been the topic of considerable research. The binding of cytochrome *c* to negatively charged phospholipid vesicles such as dioleoyl-phosphatidylglycerol (DOPG) or dimyristoylphosphatidyl-glycerol (DMPG) is governed by electrostatic interactions (Choi and Swanson, 1995; Kleinschmidt et al., 1998; Muga et al., 1991; Subramanian et al., 1998; Kostrzewa et al., 2000). However, there is also a hydrophobic interaction between the alkyl chain of the lipid and cyt-*c* (Morse and Deamer, 1973; Pinheiro, 1994; Quinn and Dawson, 1969; Salamon and Tollin, 1996a,b; Zuckermann and Heimburg, 2001).

The lysine cluster (Lys-72, Lys-86, and Lys-87) close to the exposed heme edge was believed to be a structural template common to all soluble *c*-type cytochromes. But it was shown recently that cytochrome $c_{552}$ (cyt-$c_{552}$), an electron carrier in the respiratory chain of *Thermus thermophilus*, lacks this lysine-rich domain. The region around the exposed heme edge is shielded by an additional nonpolar peptide segment that is believed to increase the thermostability of the protein (Than et al., 1997). This property of cyt-$c_{552}$ raises fundamental questions about how electron transfer occurs to its membrane bound reaction partner, as well as its own interaction with membrane. The $ba_3$-oxidase specifically recognizes the cytochrome $c_{552}$ as electron donor (Than et al., 1997) and there is no cross reactivity with the horse heart cytochrome *c*. This is due to differences in the properties of the protein surfaces interacting to form the electron transfer complex. The area around the solvent-exposed heme edge of cytochrome $c_{552}$ as well as the surface near the $Cu_A$ site of the $ba_3$-oxidase are almost uncharged. (Soulimane et al., 2000) The crystal structure of $ba_3$-oxidase shows no negatively charged residues on the putative substrate binding site, resulting in uncommon electrochemical and spectroscopic properties of the $ba_3$-oxidase (Hellwig et al., 1999). Thus the mechanism of electron transfer for cyt-$c_{552}$/$ba_3$-oxidase is different from that of cyt-*c*/cyt-*c* oxidase. Some studies have demonstrated that the main interaction between cytochrome $c_{552}$ and $ba_3$-oxidase is hydrophobic and that heterogeneous electron transfer in cyt-$c_{552}$ does not depend on a change in the heme

*Submitted March 11, 2003, and accepted for publication February 20, 2004.*

Address reprint requests to Dr. Sophie Lecomte, Laboratoire de Dynamique, Interactions et Réactivité, UMR-7075, CNRS-Université Paris VI, 2 Rue Henri Dunant, F-94320 Thais, France. Tel.: 33-1-4978-1113; Fax: 33-1-4978-1118; E-mail: sophie.lecomte@glvt-cnrs.fr.

Silke Oellerich's present address is Dept. of Biophysics, Leiden University, Niels Bohrweg 2, 2333 CA Leiden, The Netherlands.



0006-3495/04/06/3863/10 $2.00

doi: 10.1529/biophysj.103.025114

conformation, as in horse heart cyt-*c* (Lecomte et al., 1998, 1999; Bernad et al., 2003). There is no published information on the binding of cyt-$c_{552}$ to membranes or liposomes.

We therefore investigated the influence of the structure of *T. thermophilus* cyt-$c_{552}$ on its interaction with liposomes, as model membranes. We examined the binding of cyt-$c_{552}$ and cyt-*c* to DOPG vesicles to determine the similarities and differences in their behaviors. Turbidity measurements were used to evaluate the aggregation of liposomes incubated with the cytochromes. Fourier transform infrared (FTIR) spectroscopy was used to detect any changes in the secondary and tertiary structures of both proteins as they interacted with the DOPG liposomes. We also used Fourier transform infrared-attenuated total reflection (FTIR-ATR) to monitor the interaction of both proteins with a silicon surface coated with octadecyltrichlorosilane to estimate the influence of a pure hydrophobic environment on the secondary and tertiary structures of the two proteins.

## MATERIALS AND METHODS

### Proteins

Horse heart cyt-*c* was purchased from Sigma (St. Louis, MO) and used without further purification. The protein was dissolved in 5 mM HEPES, 1 mM EDTA, pH 7.6. *T. thermophilus* cyt-$c_{552}$ was isolated and purified as described previously (Soulimane et al., 1997) and dissolved in 10 mM Tris-HCl, pH 7.6.

### Vesicle preparation

DOPG was purchased from Sigma. Dry films of 10 mg lipid were prepared from a stock solution in chloroform evaporated under a stream of nitrogen and left under vacuum for at least 8 h to remove all traces of the organic solvent. The lipid films were suspended in 5 mM HEPES/EDTA, pH 7.5, or 10 mM Tris/HCl, pH 7.5, buffer and gently vortexed for a few minutes. DOPG vesicles were then prepared by sequential extrusion through polycarbonate membranes (Osmonics) of decreasing pore size (from 0.8 $\mu$m to 0.05 $\mu$m). The size of DOPG vesicles, measured by dynamic light scattering (submicron particle analyzer model N4MD, Coulter Electronics, Hialeah, FL), was ~110 nm. The DOPG vesicles used for FTIR experiments were prepared in deuterated buffer.

### Turbidity experiments

The change in the turbidity at 650 nm of the suspension of liposomes while cyt-*c* or cyt-$c_{552}$ were continuously added was recorded on a Perkin-Elmer (Foster City, CA) Lambda2 double beam spectrophotometer equipped with a temperature regulation system (Pott et al., 1998). The wavelength used was far from any electronic transition of the cytochromes. The temperature was 25°C ±0.05°C. A paddle cuvette stirrer was placed in the quartz cuvette containing the liposome suspension. The cytochrome solution was slowly and continuously injected into the cuvette through a thin tube connected to a thermostated precision glass syringe (Hamilton, Reno, NV) driven by a syringe pump (Model VI, B. Braun, Melsungen, Germany). To ensure equilibrium conditions, cyt-*c* and cyt-$c_{552}$ were injected very slowly (1.4 $\mu$L/min for 3 h) into 1.5 mL solutions with DOPG concentrations from 25 $\mu$M to 200 $\mu$M. The path length of the measuring cell was 10 mm for all experiments.

The concentration of cyt-*c* in the cuvette was deduced from the concentration of cyt-*c* in the syringe ($[\text{cyt-}c]_{\text{syringe}}$), the initial volume of the liposome suspension ($v_0$) and the added volume ($v_a$) using the equation:

$$[\text{cyt-}c]_{\text{cuvette}} = [\text{cyt-}c]_{\text{syringe}} \times v_a/(v_0 + v_a) \quad (1)$$

with

$$v_a(t) = v_{\text{syringe}} \times t/(t_{\text{tot}}), \quad (2)$$

in which $v_{\text{syringe}}$ is the total volume of the syringe, $t_{\text{tot}}$ is the time required to empty the syringe, and $t$ is the time considered during the experiment.

The lipid in the cuvette ($[\text{lip}]_{\text{cuvette}}$) was diluted; the concentration was calculated using the following equation:

$$[\text{lip}]_{\text{cuvette}} = [\text{lip}]_{\text{initial}} \times v_0/(v_0 + v_a), \quad (3)$$

in which $[\text{lip}]_{\text{initial}}$ is the initial lipid concentration in the cuvette.

### FTIR spectroscopic measurements

Deuterated buffer solutions were prepared with $K_2{}^2HPO_4$ (0.05 mol $L^{-1}$) obtained by repeated crystallization of $K_2HPO_4$ from $^2H_2O$. The $p^2H$ of all samples was adjusted by adding $^2HCl$ to obtain a value similar to pH 7.6. Lyophilized cyt-*c* and cyt-$c_{552}$ were dissolved in deuterated buffer to a final concentration of 4 mg/ml (0.32 mM for cyt-*c* and 0.28 mM for cyt-$c_{552}$). DOPG/cyt-*c* mixtures were prepared by adding DOPG vesicles in deuterated buffer to the cyt-*c* or cyt-$c_{552}$ solution. The [cyt-*c*]/[DOPG] ratio used for the FTIR experiment was selected based on the turbidity results. These experiments determined the characteristic breakpoints on the turbidity curves and thus the relationship between lipid and cytochrome concentrations. We used this relationship to set the lipid and cytochrome concentrations for the infrared experiments. The lipid-protein complexes were separated from the small amount of unbound protein by centrifugation (Beckman Coulter, Fullerton, CA) for 4 h at 4°C at 30,000 rpm (32 × *g*). The concentration of unbound protein in the supernatant was determined spectrophotometrically at 410 nm. No more than 5% of the initial protein remained in the supernatant. Control experiments with rhodamine (R6G)-labeled vesicles showed that there were no DOPG vesicles in the supernatant. Fluorescence experiments after centrifugation confirmed that there were no vesicles in the supernatant. Thus, the FTIR spectra recorded were due solely to the cytochrome/DOPG complex. The [cytochrome]/[DOPG] ratios were 0.67:10 and 1.11:10 for cyt-*c* and 0.07:10 for cyt-$c_{552}$. Protein/DOPG solutions were analyzed between two CaF2 plates of 25 $\mu$m thickness. FTIR transmission spectra were recorded with a Perkin-Elmer 1720 spectrometer (4 scans; 4 $cm^{-1}$ resolution). A Balston air dryer (Maidstone, UK) was used to reduce the water vapor content in the spectrometer. The FTIR spectra were recorded from 10 min to 5 h after sample preparation. The addition of buffer to the dry protein and protein/DOPG mixture was taken as the starting point of the processes under investigation. The FTIR spectra measured after 5 h were taken as the reference for equilibrium conditions.

### FTIR-ATR experiment

The ATR crystal was cut at 45° from monocrystalline silicon Si(100) covered with a layer of native silica. The hydrophobic silanized surface was prepared by immersing the cleaned ATR crystal in a solution of octadecyltrichlorosilane (OTS) (Roth, Strasbourg, France) as described by Wasserman et al. (1989). Briefly, the concentration of OTS was 1 mM in carbon tetrachloride/hexadecane (30:70, v/v). The wettability of the grafted self-assembled monolayers was checked by contact angle measurements using water drops. The value for OTS was 110° (Nuzzo et al., 1990). FTIR-ATR spectra were recorded on a Nicolet 850 spectrometer (Dongen, The Netherlands) with Boxcar apodization and a resolution of 4 $cm^{-1}$. The

sample compartment was continuously purged with dried air. The internal reflection element was placed in an ATR liquid cell and allowed 75 internal reflections at the liquid/crystal interface (Noinville et al., 2002). An infrared spectrum of the deuterated buffer was recorded as reference. The cell was emptied and refilled with 100 $\mu$g/mL cyt-*c* or cyt-$c_{552}$ (around 8 $\mu$M) in deuterated buffer and interferograms were recorded from 8 min to 5 h.

## Analysis of the FTIR and FTIR-ATR spectra

The spectral contributions of the buffer and adsorbents were subtracted from the measured spectra. The resulting spectra were analyzed with an algorithm based on a second derivative function and self-deconvolution procedures to determine the number and the wavenumber of individual bands within the spectral range 1500–1750 $cm^{-1}$ (Fig. 1; see also Boulkanz et al., 1997; Lecomte et al., 2001). The relative contributions of the various bands were obtained by a band-fitting procedure, keeping the wavenumbers, half widths at half heights (14–20 $cm^{-1}$), and band profiles (75% Gaussian and 25% Lorentzian) constant and allowing only the intensities to vary. All spectra could be fitted by seven amide I' and two amide II components along with a few bands assigned to amino acid side chains. The content of the various secondary-structure elements was estimated by dividing the integral intensity of one amide I' band component by the total intensity of all amide I' band components. The amount of each secondary-structure element is given as a percentage. The surface of the amide I' band was considered to be due only to the amide I' band of the polypeptide backbone, neglecting the amide groups of the Gln and Asp side chains. The *T. thermophilus* cyt-$c_{552}$ contains 3 Asn and 10 Gln residues, whereas horse heart cyt-*c* has only five Asn and three Gln. All are exposed to the solvent, so the amide I' wave numbers should be 1650 for Asn and 1635 $cm^{-1}$ for Gln residues (Chirgadze et al., 1975; Sukhishvili and Granick, 1999), with molar extinction coefficients comparable to those of the polypeptide backbone (Chirgadze et al., 1975). These bands were not included in the band-fitting analysis, so that the relative contributions of the amide I′ band components indicating peptide bonds in random-coil domains (1638 $cm^{-1}$) and $\beta$-strands or turns (1630 $cm^{-1}$) and in the $\alpha$-helix (1660 and 1646 $cm^{-1}$) were overestimated. The contribution of the Asn/Gln side chains to the amide I′ band was constant in all spectra recorded; thus, the error of the secondary-structure determination is constant and systematic. The intensity redistribution among the amide I′ bands can be quantified in terms of secondary-structure changes, allowing for the numbers of peptide bonds in cyt-*c* (Buschnell et al., 1990) and cyt-$c_{552}$ (Than et al., 1997). Thus, a 2% increase or decrease in amide I′ integrated absorbance is due to 2–3 peptide bonds. The integral amide II band intensities were normalized in the same way. The amide II/amide I′ integrated absorbance ratio was used to assess the degree of $H/^2H$ exchange using a reference value of 0.5 for totally hydrogenated proteins in the solid state, according to studies of various globular proteins in solid state.

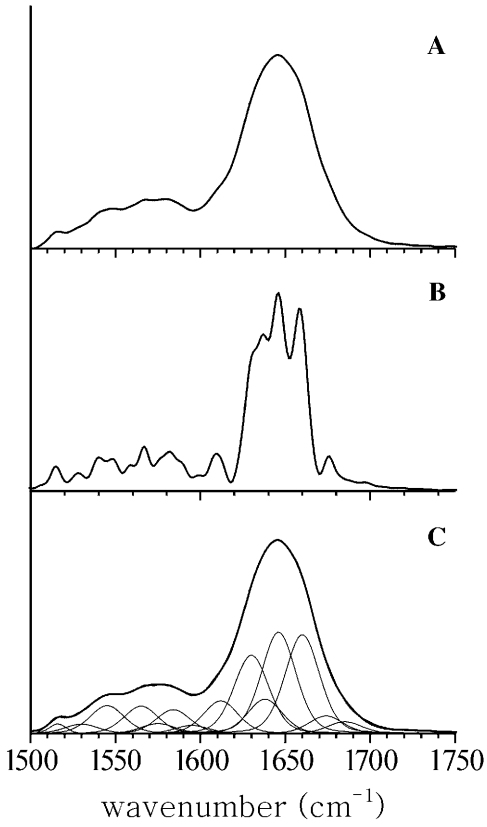


FIGURE 1 FTIR spectra of cyt-$c_{552}$ in deuterated buffer (pD 8). (*A*) Experimental spectrum obtained after subtracting the buffer contribution. (*B*) Spectrum showing individual band components obtained from second-derivative analysis. (*C*) Experimental spectrum including the band components.

# RESULTS

## Turbidity experiments

The change in liposome turbidity during the continuous injection of cyt-*c* or cyt-$c_{552}$ was recorded (Figs. 2 and 3). The turbidity curves were characteristic for each *c*-type cytochrome and similar in shape, whatever the initial lipid concentration. However, the curves were shifted toward higher cytochrome concentrations when the lipid concentration was increased. This indicates that the phenomenon revealed by the change in turbidity depended on the lipid and the cytochrome concentrations. The turbidity curves for cyt-*c* showed four reproducible breakpoints determined by the intercept of the tangents (Fig. 2 *B*), whereas those for cyt-$c_{552}$ showed only two breakpoints (Fig. 3 *B*). The total protein concentrations at which each of those breakpoints was reached varied linearly with the DOPG concentration (Fig. 4). According to Pott et al. (1998), the equations for the linear relationships can be written as:

$$[\text{cyt-}c]_{\text{tot}} = [\text{cyt-}c]_{\text{u}} + R^* [\text{Lip}]_{\text{tot}}, \quad (4)$$

in which $[\text{cyt-}c]_{\text{tot}}$ is the total cyt-*c* concentration, $[\text{cyt-}c]_{\text{u}}$ is the unbounded cyt-*c* concentration not bound to lipid, given by the intercept, $R^*$ is the $[\text{cyt-}c]_{\text{lip}}/[\text{Lip}]_{\text{tot}}$ ratio, where $[\text{cyt-}c]_{\text{lip}}$ is the cyt-*c* concentration interacting with the lipids and $[\text{Lip}]_{\text{tot}}$ the total lipid concentration. According to this equation, the $R^*$ value for each breakpoint is given by the slope of the straight line and the free cytochrome concentration is obtained by extrapolating the straight line to zero lipid concentration (Table 1). The concentrations of free cytochrome in solution were low, indicating that both proteins were bound strongly to the DOPG vesicles. In contrast, the $R^*$ required for aggregation of liposomes by horse heart cyt-*c* was almost one order of magnitude higher than that for *T. thermophilus* cyt-$c_{552}$ (see Table 1).

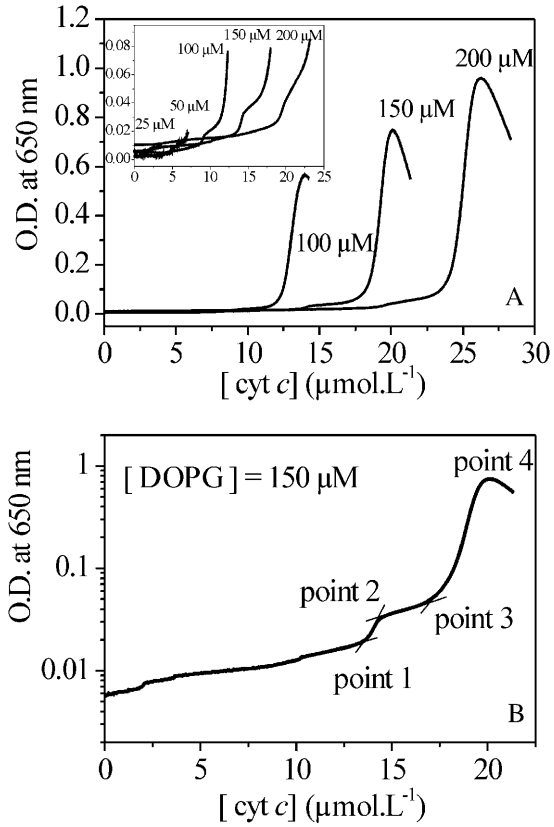


FIGURE 2 Optical density was recorded at 650 nm, while adding cyt-*c* to 25, 50, 100, 150, and 200 $\mu$M of DOPG in 5 mM HEPES,1 mM EDTA buffer, pH 7.6 (*A*). Detail of one curve to show the breakpoints (*B*).

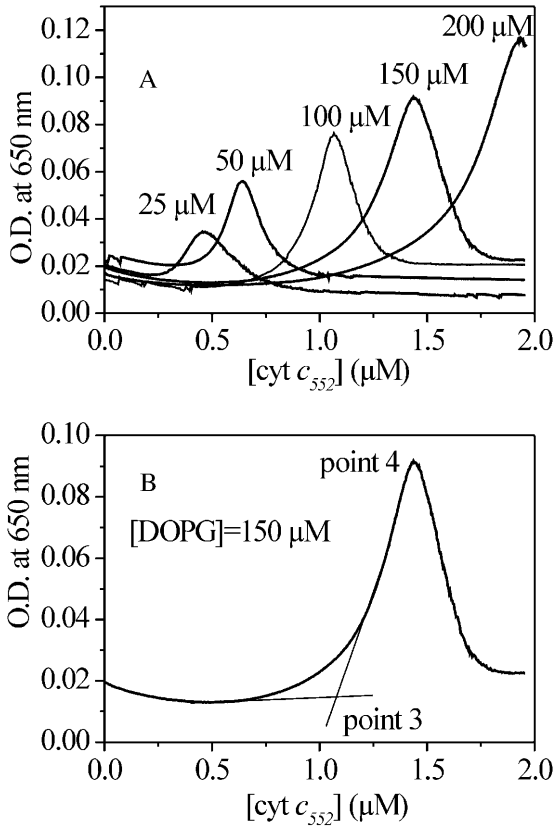


FIGURE 3 Optical density was recorded at 650 nm, while adding cyt-$c_{552}$ to 25, 50, 100, 150, and 200 $\mu$M of DOPG in 10 mM Tris-HCl, pH 7.6 (*A*). Detail of one curve to show the breakpoints (*B*).

The two first breakpoints for cyt-*c* were reached for very similar *R** values (0.94:10 and 0.98:10), whereas the *R** corresponding to the beginning of aggregation (point 3) was 1.17:10 and the *R** for macroscopic flocculation (point 4) was 1.22:10. A simple calculation, assuming that the available surface area of one cyt-*c* molecule is 910 Å$^2$ (Buschnell et al., 1990) and the surface area of the DOPG head group is 80 Å$^2$, indicated that a monolayer of cytochrome *c* surrounds the DOPG vesicle, corresponding to a *R** value of 0.5:10. Therefore, cyt-*c* forms a second bound layer from the first experimental breakpoint. The great increase in turbidity at breakpoint 3 is probably due to the beginning of aggregation of the cyt *c*-loaded DOPG vesicles. The last breakpoint is due to the sedimentation of the liposome-cyt complexes visible macroscopically, explaining the decrease in the optical density at 650 nm. A similar aggregation occurs with DMPG liposomes (De Meulenaer et al., 1997; Paquet et al., 2001). By two-dimensional infrared correlation, Paquet et al., 2001 suggested that aggregation starts to occur between nearly native proteins, which then unfold, resulting in further aggregation.

The effect of cyt-$c_{552}$ binding to DOPG vesicles is quite different, as revealed by the shape of the turbidity curve and by the different *R** values at flocculation. We again estimated the surface area ratio cyt-$c_{552}$/DOPG at the flocculation point, assuming that the available surface area of one cyt-$c_{552}$ molecule was 1400 Å$^2$ (Than et al., 1997) and found 0.145, which was very low, and indicated that aggregation takes place when the liposome surface is far from covered by absorbed protein. Cyt-$c_{552}$ is also positively charged at physiological pH, but the distribution of the charge is quite different from that for the eukaryote cytochrome *c*.

## FTIR-experiments on cyt-*c* and cyt-$c_{552}$ in deuterated buffer

The 1600–1700 cm$^{-1}$ spectral region is dominated by the amide I' mode of the polypeptide backbone of cytochrome. A large number of experimental data enabled us to assign the individual amide I' band components to various elements of proteins secondary structure (Byler and Susi, 1986; Surewicz and Mantsch, 1988). Table 2 summarizes the assignment of the components of the amide I' band of both cytochromes. The assignment of the amide I' band of the *T. thermophilus* cyt-$c_{552}$ has been already described and discussed (Lecomte et al., 2001). Several assignments have been reported for horse heart cyt-*c* (Byler and Susi, 1986; Lo and Rahman,

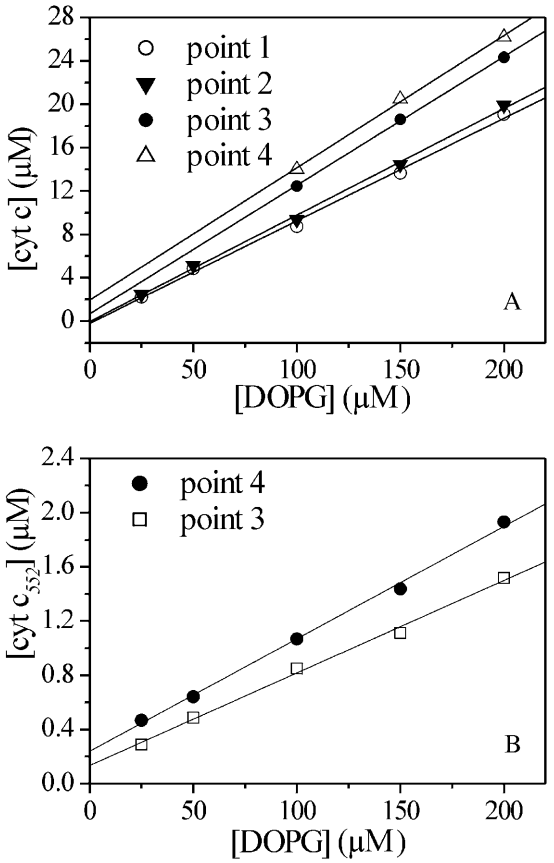


FIGURE 4 Linear relationship between the total protein concentration and the DOPG concentration at each breakpoint. (*A*) cyt-*c*; (*B*) cyt-$c_{552}$.

1998; Paquet et al., 2001). Except for the assignment of the band at 1660 $cm^{-1}$, described by Heimburg and Marsh (1993) and Lo and Rahman (1998) as a contribution to the amide I' group involved in $\beta$-turns, the assignment in Table 2 is in a good agreement with those of other authors (Goormaghtigh et al., 1990; Dong et al., 1992). However, the difference may arise because the authors (Heimburg and Marsh, 1993; Lo and Rahman, 1998) used only six bands for the self-decomposition of the amide I' bands and because the half-width of the band associated with an $\alpha$-helix is large. From their analysis the calculated percentage of $\alpha$-helix is very different from the value determined by x-ray crystallography. The crystal structures of cyt-*c* and cyt-$c_{552}$ show

**TABLE 1 Characteristic points of the turbidity changes for binding of cyt-*c* or cyt-$c_{552}$ to DOPG vesicles**

| | cyt-*c* | | cyt-$c_{552}$ | |
|---|---|---|---|---|
| Breakpoints | $[cyt]_{unbound}$ ($\mu$M) | *R** ($\mu$M/$\mu$M) | $[cyt]_{unbound}$ ($\mu$M) | R* ($\mu$M/$\mu$M) |
| 1 | 0 | 0.94:10 | | |
| 2 | 0 | 0.98:10 | | |
| 3 | 1.658 | 1.17:10 | 0.133 | 0.07:10 |
| 4 | 1.921 | 1.22:10 | 0.237 | 0.08:10 |

**TABLE 2 Assignment of the infrared bands of *T. thermophilus* cyt-$c_{552}$ and horse heart cyt-*c***

| Mode | cyt-$c_{552}$* | cyt-*c* | |
|---|---|---|---|
| Amide I | 1697 | 1697 | $\beta$-strands in apolar domains |
| | 1676 | 1676 | Nonhydrogen-bonded inside the protein core |
| | 1660 | 1660 | Hydrogen-bonded in irregular/internal $\alpha$-helix |
| | 1646 | 1652 | Hydrogen-bonded in regular/external $\alpha$-helix |
| | 1638 | 1641 | Hydrated in random domains |
| | 1630 | 1630 | Hydrogen-bonded in $\beta$-strands or turns |
| | 1612 | 1616 | Hydrogen-bonded in protein self-association |
| Amide II | 1545 | 1546 | Strongly hydrogen-bonded NH |
| | 1530 | 1530 | Weakly hydrogen-bonded NH |

Wave numbers refer to bands determined by second derivative analysis (FTIR).
*For assignments see Lecomte et al. (2001).

that ~45% and 49% of the amino acids are involved in an $\alpha$-helix (Buschnell et al., 1990; Than et al., 1997), which is in good agreement with the relative contributions (%) of each secondary structure element determined by our analysis of the FTIR spectra (see Tables 3 and 4). The profiles of the amide I' bands in the two cytochromes were different, in agreement with their structures. Cyt-$c_{552}$, which is more compact and more hydrophobic than cyt-*c*, has 16% fewer residues involved in the hydrated random domain than cyt-*c*) and more residues in internal or hydrophobic $\alpha$-helices (+6%) or $\beta$-turn structures (+6%). The analysis of the FTIR

**TABLE 3 Secondary-structure elements and NH contents (in %) of horse heart cyt-*c* dissolved in deuterated buffer and cyt-*c* in the presence of DOPG vesicles or adsorbed onto an OTS surface**

| | Relative contribution (%)* | | | |
|---|---|---|---|---|
| Secondary-structure element | cyt-*c*† | [cyt-*c*]/[DOPG]‡ 0.66:10 | 1.11:10 | cyt-*c* + OTS¶ |
| $\beta$-strands in nonpolar domains | 0 | 0 | 0 | 0 |
| Nonhydrogen-bonded inside the protein core | 10 | 10 | 11 | 11 |
| Hydrogen-bonded in irregular/internal $\alpha$-helix | 20 | 19 | 18 | 18 |
| Hydrogen-bonded in external/regular $\alpha$-helix | 24 | 26 | 26 | 14 |
| Hydrated in random domains | 27 | 26 | 26 | 29 |
| Hydrogen-bonded in $\beta$-strands or turns | 14 | 14 | 14 | 18 |
| Hydrogen-bonded in protein self-association | 5 | 5 | 5 | 10 |
| % NH* | 15% | 8% | | 3% |

*Percentages determined from the FTIR spectra measured after 5 h.
†Cyt-*c* (4 mg/mL) in deuterated buffer.
‡DOPG vesicles (3.85 and 2.5 mg/mL) in deuterated buffer is added to solution of cyt-*c* (4mg/mL), giving [cyt-*c*]/[DOPG] ratios of 0.66:10 and 1.11:10.
¶Cyt-*c* (100 $\mu$g/mL) for FTIR-ATR experiment.

**TABLE 4 Secondary-structure elements and NH contents (in %) of *T. thermophilus* cyt-$c_{552}$ dissolved in deuterated buffer and of cyt-$c_{552}$ in the presence of DOPG vesicles or adsorbed onto an OTS surface**

| Secondary-structure element | Relative contribution (%)* | | |
|---|---|---|---|
| | cyt-$c_{552}$[†] | cyt-$c_{552}$ + DOPG[‡] | cyt-$c_{552}$ + OTS[¶] |
| $\beta$-strands in nonpolar domains | 2 | 3 | 1 |
| Nonhydrogen-bonded inside the protein core | 8 | 8 | 6 |
| Hydrogen-bonded in irregular/internal $\alpha$-helix | 26 | 26 | 20 |
| Hydrogen-bonded in external/regular $\alpha$-helix | 25 | 24 | 27 |
| Hydrated in random domains | 11 | 8 | 5 |
| Hydrogen-bonded in $\beta$-strands or turns | 20 | 21 | 30 |
| Hydrogen-bonded in protein self-association | 8 | 10 | 11 |
| % NH* | 25% | 17% | 8% |

*Percentages determined from the FTIR spectra measured after 5 h.
[†]Cyt-$c_{552}$ (4 mg/mL) in deuterated buffer.
[‡]DOPG vesicles (16 mg/mL) in deuterated buffer added to a solution of cyt-$c_{552}$ (2 mg/mL), giving a [cyt-$c_{552}$]/[DOPG] ratio of 0.07:10.
[¶]Cyt-$c_{552}$ (100 $\mu$g/mL) for FTIR-ATR experiment.

spectra of both cytochromes at different times after dissolution gave similar results for the secondary-structure elements (result not shown).

The analysis of the 1600–1500 $cm^{-1}$ spectra showed the contributions of eight components reflecting the vibration modes of some side chain of amino acid residues plus the amide II modes. The amide II mode involves the NH in-plane bending mode and disappears upon H/$^2$H exchange. Thus the total integrated absorbance of the amide II bands is appropriate for monitoring the H/$^2$H exchange of a protein dissolved in $^2H_2O$. This mode was assigned to the bands at 1530 and 1546 $cm^{-1}$, corresponding to weakly and strongly hydrogen-bonded amide groups (Baron et al., 1978). The analysis of the amide II band showed that 80% of the amide groups of cyt-*c* were deuterated 10 min after dissolution and 85% after 5 h. The amide bonds that remained hydrogenated were obviously buried in the core of the protein and hence, less accessible to the solvent. The percentage of exchanged amide groups was lower for cyt-$c_{552}$; it varied from 60% at 10 min to 75% at 5 h. The presence of more hydrophobic residues on the external surface of the protein plus the large $\beta$-turn covering the heme could prevent water penetrating, hence the smaller NH/N$^2$H exchange for cyt-$c_{552}$ than for cyt-*c*.

## Binding of cyt-*c* and cyt-$c_{552}$ to DOPG vesicles

The components used for the spectral analysis of the FTIR spectra of the cytochrome/DOPG mixtures were identical to those for cyt-*c* and cyt-$c_{552}$ in solution; only the integrated absorbance of the band was varied. The diagram in Fig. 5 *A* shows the percentages of amide groups involved in secondary structure elements in cyt-*c* in solution and cyt-*c* bound to DOPG vesicles at a [cyt-*c*]/[DOPG] ratio of 1.1:10 (after breakpoint 2). The values in Table 3 show the result for a [cyt-*c*]/[DOPG] ratio of 0.66:10 (before breakpoint 1). The secondary structure elements underwent only small changes when the protein was bound to DOPG vesicles at all the [cyt-*c*]/[DOPG] ratios used. This is in agreement with published data (Choi and Swanson, 1995; Heimburg and Marsh, 1993). There is only a small decrease (−2%) in the 1660 $cm^{-1}$ component that is assigned to peptide bonds in an internal $\alpha$-helix, with an increase (+2%) in the amide I' involved in the external $\alpha$-helix, but a 2% change is close to the repeatability error of the experiment (Lecomte et al., 2001). On the other hand, the adsorption of cyt-*c* on DOPG vesicles

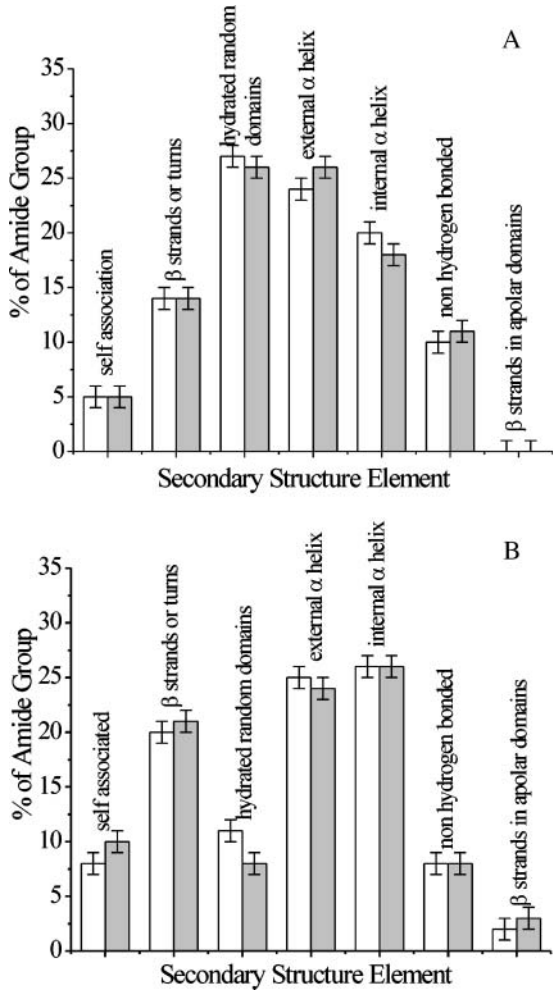


FIGURE 5 (*A*) Percentage of cyt-*c* amide I' groups involved in secondary-structure elements: white, cyt-*c* (4 mg/mL) in deuterated buffer; light gray, cyt-*c* bound to DOPG vesicles. (*B*) white, cyt-$c_{552}$ (4 mg/ml) in deuterated buffer; light gray, cyt-$c_{552}$ bound to DOPG vesicles.

increased the H/$^2$H exchange, since 92% of the NH groups of cyt-*c* bound to DOPG vesicles were exchanged after 5 h.

The [cyt-$c_{552}$]/[DOPG] ratio used for the FTIR analysis corresponded to the $R^*$ value of 0.07:10. The data for cyt-$c_{552}$ amide I' bound to DOPG vesicles are listed in Table 4. The spectra were very similar to those for cyt-$c_{552}$ in solution (Fig. 5 *B*). The only significant change in % amide I' was a slight decrease (−3%) in the 1638 cm$^{-1}$ component, attributable to peptide bonds in hydrated random domains. But the tertiary structure of the cyt-$c_{552}$ was modified, as revealed by the variation of amide II band: the NH/N$^2$H exchange for the bound cyt-$c_{552}$ was 8% greater than for cyt-$c_{552}$ in solution. The final residual percentage of NH (17%) was still higher than for cyt-*c* (8%), reflecting the more compact, stable structure of the *T. thermophilus* cytochrome.

### Binding of cyt-*c* and cyt-$c_{552}$ to a hydrophobic surface

cyt-*c* was deposited on self-assembled monolayers of alkylsilanes on silicon to determine the change in cyt-*c* structure that occurred when it was adsorbed onto a pure hydrophobic surface. Fig. 6 *A* shows the difference between the secondary structure of a monolayer of cyt-*c* adsorbed onto the hydrophobic OTS surface and that of cyt-*c* in solution. The changes were much greater than those involved in binding to DOPG vesicles (see Table 3). The adsorption onto an alkyl chain drastically modified the amide groups involved in $\alpha$-helix structures. Forty-four percent of the amide groups in solvated cyt-*c* were involved in internal or external $\alpha$-helix structures, but only 32% of them were involved in $\alpha$-helices when the protein was adsorbed onto OTS, with more amino acids implicated in $\beta$-turns (+4%) or in protein self association (+5%) and in random domains (+2%). These changes involved at least 12% of the backbone, corresponding to 10–12 residues. The percentage of residual NH of cyt-*c* adsorbed onto the OTS surface after 5 h was also very small (3%) compared to 15% of residual NH for cyt-*c* in solution. Most of the amide groups were exchanged by $^2H_2O$, indicating a large change in the tertiary structure of the protein. Thus the adsorption of cyt-*c* onto alkyl chains modifies its secondary and tertiary structures, resulting in the spreading of cyt-*c* adsorbed onto the hydrophobic surface because of unfolding of the protein and increased self-association.

The changes in secondary structure of cyt-$c_{552}$ adsorbed onto the hydrophobic OTS surface under equilibrium conditions are shown in Fig. 6 *B* and Table 4. The band intensity at 1630 cm$^{-1}$ increased from ~20–30%, whereas the band intensities at 1660 cm$^{-1}$ and 1638 cm$^{-1}$ decreased to 6%. At least 15% of the peptide backbone of cyt-$c_{552}$ was modified by adsorption onto OTS. These changes can be attributed to the formation of $\beta$-strand/turn structures, unfolding of part of the $\alpha$-helix structure and a loss of hydrated random-coil domains. Analysis of the amide II bands indicated that the tertiary structure of the cyt-$c_{552}$ was greatly altered when it was adsorbed onto alkyl chains. The adsorption allows the diffusion of $^2H_2O$ into buried domains, as reflected by the low final percentage of residual NH (8%).

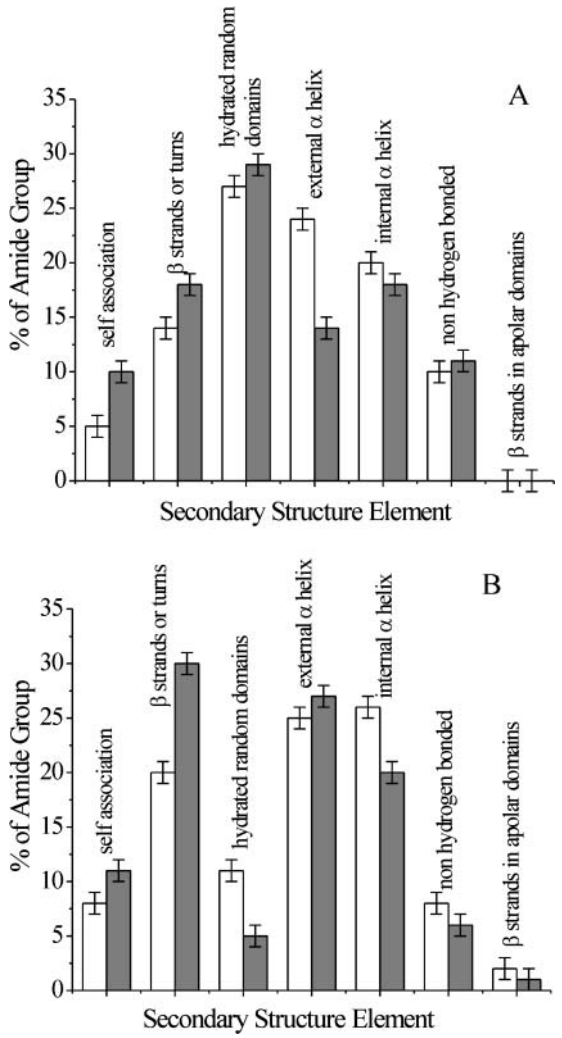


FIGURE 6 Percentage of cyt-$c_{552}$ amide I' group involved in secondary-structure elements. (*A*) White, cyt-*c* (4 mg/ml) in deuterated buffer; dark gray, cyt-*c* (100 $\mu$g/ml) adsorbed onto OTS surface. (*B*) White, cyt-$c_{552}$ (4 mg/ml) in deuterated buffer; dark gray, cyt-$c_{552}$ (100 $\mu$g/ml) adsorbed onto an OTS surface.

## DISCUSSION

Both the horse heart and *T. thermophilus* cytochromes bind strongly to DOPG vesicles at low ionic strength. Although the turbidity experiments generally demonstrate that they bind to the liposomes, they also show that the binding of cyt-*c* differs from that of cyt-$c_{552}$. Multilayers of cyt-*c* seem to be adsorbed onto DOPG, resulting in aggregation of the protein. The formation of the multilayer causes flocculation and sedimentation. Flocculation and

sedimentation appear when very little of the DOPG vesicle surface is covered by cyt-$c_{552}$. The monolayer is incomplete. The interaction between one molecule of cyt-*c* and eight molecules of DOPG leads to sedimentation, whereas 120 molecules of DOPG are necessary to obtain sedimentation with cyt-$c_{552}$. The net charges of the two cytochromes are similar in the buffer used, +9 for cyt-*c* and +7 for cyt-$c_{552}$. Although the neutralization of charges can explain the sedimentation with cyt-*c*, it cannot do so for cyt-$c_{552}$, flocculation of which occurs at a much higher lipid/cytochrome ratio than the theoretical neutralization ratio of 9:7.

The nature of the interactions between eukaryotic *c*-type cytochrome and DOPG vesicles has been described by several authors (De Meulenaer et al., 1997; Heimburg and Marsh, 1993; Morse and Deamer, 1973; Muga et al., 1991; Quinn and Dawson, 1969). The forces driving the interaction of the eukaryotic cyt-*c* and negatively charged lipid are mainly electrostatic (Kostrzewa et al., 2000; Muga et al., 1991; Salamon and Tollin, 1996a). Such an electrostatic interaction between the positively charged residues and the negatively charged headgroups of DOPG explains the strong binding of cyt-*c* to DOPG. The horse heart cyt-*c* has the typical positively charged front surface, in which a cluster of lysine residues surround the exposed heme edge (Buschnell et al., 1990) (see Fig. 7 *A*). Cytochrome *c* seems to bind to the DOPG vesicles via the heme side of the protein. A recent paper has demonstrated that Lys-86, Lys-87, and Lys-72 are involved in the cyt *c*-membrane (DOPG) interaction (Kostrzewa et al., 2000). However, some authors have reported that cytochrome *c* can also become inserted into the lipid bilayer of DOPG vesicles (Cortese et al., 1998; Pinheiro and Watt, 1994; Zuckermann and Heimburg, 2001). The FTIR-ATR experiments were performed to determine how the secondary structures of the two cytochromes interact with a hydrophobic solid surface. The secondary structure of horse heart cytochrome *c* changes greatly, mainly due to unfolding of $\alpha$-helix to form hydrated $\beta$-strands or turns associated with the high degree of NH/N$^2$H exchange. The rate of cyt-*c* adsorption onto the OTS surface reveals that a compact monolayer of cyt-*c* molecules is formed (results not shown). The protein also aggregates, as revealed by the increase in the band at 1616 cm$^{-1}$. All of these modifications are corroborated by the high degree of NH/N$^2$H exchange and indicate considerable denaturation of the cyt-*c* adsorbed onto the hydrophobic surface. Although it is quite difficult to define a specific binding domain on the original structure, two external $\alpha$-helices (Val-3 and Gly-6; Phe-10 and Lys-13) containing hydrophobic residues could be implicated in the interaction with the hydrophobic surface. The orientation of these two fragments toward the absorbent surface causes a loss of $\alpha$-helix. The extensive unfolding of cyt-*c* adsorbed onto the hydrophobic surface is consistent with a majority of a nonnative forms (5cHS) of the heme detected by surface-enhanced resonance Raman spectroscopy (Rivas et al., 2002).

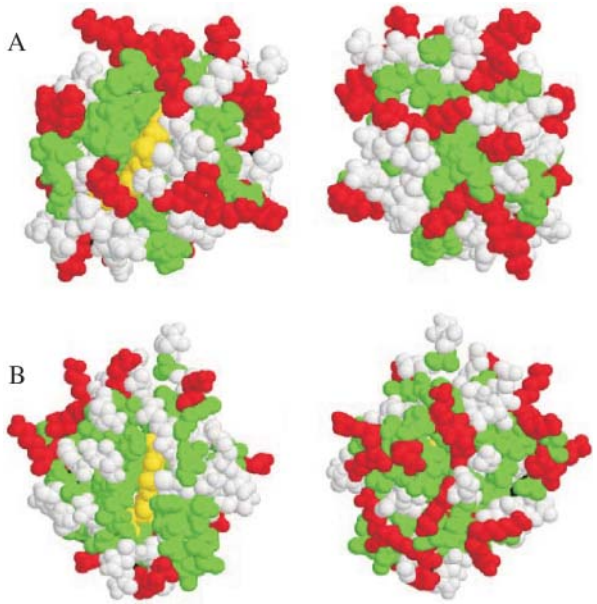


FIGURE 7 Space-filling plot of the structures of cyt-*c* (*A*) and cyt-$c_{552}$ (*B*). Lysine and arginine residues are shown in red and hydrophobic residues in green. *Right*: View of the front side including the heme site (*yellow*); *left*: view of the back side of the heme. The figures were prepared with the program RASMOL.

The adsorption of cyt-*c* onto DOPG vesicles produces only changes in the tertiary structure of cyt-*c*, without any change in the secondary structure, except that the protein penetrates deep into the hydrophobic core of the bilayer. However, partial insertion of the protein into the bilayer and the formation of hydrophobic contacts cannot be completely ruled out. A resonance Raman experiment with cyt-*c* adsorbed onto DOPG vesicles indicates that there are various heme structures, which implies the presence of hydrophobic interactions between cyt-*c* and DOPG vesicles in addition to the electrostatic interactions (Oellerich et al., 2004).

Cyt-$c_{552}$ also has a strong affinity for DOPG vesicles, but the structure of this protein differs from that of eukaryotic cytochrome *c*. Cyt-$c_{552}$ has only uncharged residues around the exposed heme edge, unlike a typical *c*-type cytochrome (Than et al., 1997) (see Fig. 7 *B*). The lysine and arginine residues are located on the back side of the heme, where several carbonyl side chains are also situated, creating negative potential at the center, top, and bottom of the back side. The binding of cyt-$c_{552}$ on DOPG vesicles can be also explained by electrostatic interaction between the lysine residues and the negatively charged headgroups of the lipid. The exposed heme edge is surrounded by many hydrophobic residues and this part of the protein is almost totally uncharged (Fig. 7 *B*). The adsorption of cyt-$c_{552}$ onto a purely hydrophobic surface also results in major changes in its secondary structure, but they are different from the changes undergone by cyt-*c*. The global content of structured regular domains is increased by 4% with the formation of $\beta$-structures. The secondary structure of cyt-$c_{552}$ adsorbed

onto talc undergoes similar changes (Lecomte et al., 2001). The specific orientation of the cyt-$c_{552}$ adsorbed onto hydrophobic surfaces occurs without the protein spreading. This is consistent with the low content of self-associated domains (band at 1616 $cm^{-1}$; Table 4); they are quite similar in cyt-$c_{552}$ in solution and the protein adsorbed onto DOPG vesicles or the OTS. The domains that are modified by the hydrophobic surface are different from those involved in horse heart cyt-*c*. The crystal structure of cyt-$c_{552}$ reveals two hydrophobic regions on the front surface close to the heme (Than et al., 1997). These are both candidates for the interaction with OTS surface. One domain involves the hydrophobic $\beta$-strands (Gly-19–Pro-27) close to the enlarged $\beta$-strands (Met-63–Leu-75) and the second is the N-terminal helix (Ala-2–Ala-9). This terminal peptide segment includes several alanine and isoleucine residues which can easily be oriented toward the hydrophobic OTS surface. The N-terminal segment is close to the reserved Met-63–Leu-75 $\beta$-strand and includes an $\alpha$-helical portion which, if it changed to a $\beta$-sheet, would contribute to the formation of a more extended $\beta$-sheet domain. These changes in secondary structure could account for the increase in $\beta$-sheet at the expense of $\alpha$-helical structure that occurs when the protein binds to the OTS surface. The opening of the $\beta$-strand could also explain the large exchange of NH/$N^2$H. The secondary structure of cyt-$c_{552}$ bound to DOPG vesicles does not seem to change much, according to the FTIR experiments. The change is much less than that occurring when the protein is bound to a pure hydrophobic surface. However, a purely electrostatic interaction with DOPG vesicles cannot explain the great aggregation that occurs at a low *L*/*P* ratio. This could imply that cyt-$c_{552}$ also becomes inserted into bilayers via hydrophobic interactions. The hydrophobic $\beta$-sheet surrounding the heme may act as an anchor in the vesicle. This local interaction involving a few amino acid residues would not be detected by the global FTIR analysis. The very small changes occurring when cyt-$c_{552}$ is adsorbed onto DOPG vesicles are at the limit of the accuracy of our method. The positively charged residues can still interact with the negatively charged phosphatidyl headgroups via electrostatic interaction. The coexistence of electrostatic and hydrophobic interactions could explain the low cyt-$c_{552}$/DOPG ratio at which flocculation occurs. Cyt-$c_{552}$ could form bridges between DOPG vesicles.

## CONCLUSION

Both horse heart cytochrome *c* and *T. thermophilus* cyt-$c_{552}$ have high affinities for DOPG vesicles at low ionic strength. The two type *c* cytochromes both bind to DOPG vesicles without any change in their secondary structures and the only change in their tertiary structures is that both cytochromes become more open.

However, the turbidity experiments detected differences in their behavior when binding to DOPG vesicles; the cytochrome *c* formed multilayers on the surface of the DOPG vesicles, whereas the cyt-$c_{552}$ caused the DOPG vesicles to aggregate even when their surfaces were not completely covered by protein. These features show the different stabilities of the two cytochromes in their interactions with DOPG vesicles. The binding of cyt-*c* to DOPG vesicles involves mainly electrostatic interactions. Cyt-*c* is greatly unfolded when it is adsorbed onto a purely hydrophobic surface, so there are hydrophobic interactions or cyt-*c* becomes inserted into the liposome. In contrast, the binding of cyt-$c_{552}$ to DOPG vesicles is more complex. Electrostatic interactions cannot solely explain the extensive aggregation of DOPG vesicles covered by only a few molecules of protein. However, a purely hydrophobic interaction during cyt-$c_{552}$ binding should cause more folding in a $\beta$-structure. The spectral features of cyt-$c_{552}$ adsorbed onto DOPG vesicles are similar to those seen when it is adsorbed onto hydrophobic surface, but this does not exclude hydrophobic interactions or maintain their prevailing with respect to electrostatic ones. The interactions of cytochrome *c* and cytochrome $c_{552}$ with charged lipid membranes and hydrophobic surfaces are different, raising the question of how the functions of the two proteins differ.

## REFERENCES


Baron, M. H., C. De Loze, C. Toniolo, and C. D. Fasman. 1978. Structure in solution of protected homo-oligopeptides of L-valine, L-isoleucine, and L-phenylalanine: an infrared adsorption study. *Biopolymers.* 17:2225–2239.

Bernad, S., T. Soulimane, and S. Lecomte. 2004. Redox and conformational equilibria of cytochrome $c_{552}$ from *Thermus thermophilus* adsorbed on chemically modified silver electrode probed by surface enhanced resonance Raman spectroscopy. *J. Raman Spectr.* 35:47–54.

Boulkanz, L., N. Balcar, and M. H. Baron. 1995. FT-IR analysis for structural characterization of albumin adsorbed on the reversed-phase support RP-$C_6$. *Appl. Spectr.* 49:1737–1746.

Boulkanz, L., C. Vidal-Madjar, N. Balcar, and M. H. Baron. 1997. Adsorption mechanism of human serum albumin on a reversed-phase support by kinetic, chromatographic, and FTIR method. *J. Coll. Interf. Sci.* 188:58–67.

Buschnell, G. W., G. V. Louie, and G. D. Brayer. 1990. High-resolution three-dimensional structure of horse heart cytochrome c. *J. Mol. Biol.* 214:585–595.

Byler, D. M., and H. Susi. 1986. Examination of the secondary structure of proteins by deconvolved FTIR spectra. *Biopolymers.* 25:469–487.

Chirgadze, Y. N., O. V. Fedorov, and N. P. Trushina. 1975. Estimation of amino acid residue side-chain absorption in the infrared spectra of protein solutions in heavy water. *Biopolymers.* 14:679–694.

Choi, S., and J. M. Swanson. 1995. Interaction of cytochrome c with cardiolipin: an infrared spectroscopic study. *Biophys. Chem.* 54:271–278.

Cortese, J. D., A. L. Voglino, and C. R. Hackenbrock. 1998. Multiple conformations of physiological membrane-bound cytochrome c. *Biochemistry.* 37:6402–6409.

De Meulenaer, B., P. Van der Meeren, M. De Cuyper, J. Vanderdeelen, and L. Baert. 1997. Electrophoretic and dynamic light scattering study of the interaction of cytochrome *c* with dimyristoylphosphatidylglycerol, dimyristoylphosphatidylcholine, and intramembranously mixed liposomes. *J. Coll. Interf. Sci.* 189:254–258.

Dong, A., P. Huang, and W. S. Caughed. 1992. Redox-dependent changes in $\beta$-extended chain and turn structures of cytochrome c in water solution

determined by second derivative amide I infrared spectra. *Biochemistry.* 31:182–189.

Goormaghtigh, E., V. Cabiaux, and J. M. Ruysschaert. 1990. Secondary structure and dosage of soluble and membrane proteins by attenuated total reflection Fourier-transform infrared spectroscopy on hydrated films. *Eur. J. Biochem.* 193:409–420.

Heimburg, T., and D. Marsh. 1993. Investigation of secondary and tertiary structural changes of cytochrome *c* in complexes with anionic lipids using amide hydrogen exchange measurements: an FTIR study. *Biophys. J.* 65:2408–2417.

Hellwig, P., T. Soulimane, G. Buse, and W. Mantele. 1999. Electrochemical, FTIR, and UV/VIS spectroscopic properties of the $ba_3$ oxidase from *Thermus thermophilus*. *Biochemistry.* 38:9648–9658.

Kleinschmidt, J. H., G. L. Powell, and D. Marsh. 1998. Cytochrome *c*-induced increase of motionally restricted lipid in reconstituted cytochrome c oxidase membranes, revealed by spin-label ESR spectroscopy. *Biochemistry.* 37:11579–11585.

Kostrzewa, A., T. Pali, W. Froncisz, and D. Marsh. 2000. Membrane location of spin-labeled cytochrome c determined by paramagnetic relaxation agents. *Biochemistry.* 39:6066–6074.

Lecomte, S., P. Hildebrandt, and T. Soulimane. 1999. Dynamics of the heterogeneous electron-transfer reaction of cytochrome $c_{552}$ from *Thermus thermophilus*. A time-resolved surface-enhanced resonance Raman spectroscopic study. *J. Phys. Chem. B.* 103:10053–10064.

Lecomte, S., C. Hilleriteau, J. P. Forgerit, M. Revault, M. H. Baron, P. Hildebrandt, and T. Soulimane. 2001. Structural changes of cytochrome $c_{552}$ from *Thermus thermophilus* adsorbed on anionic and hydrophobic surfaces probed by FTIR and 2D-FTIR spectroscopy. *Chem. Biochem.* 2:180–189.

Lecomte, S., H. Wackerbarth, T. Soulimane, G. Buse, and P. Hildebrandt. 1998. Time-resolved surface-enhanced resonance Raman spectroscopy for studying electron-transfer dynamics of heme proteins. *J. Am. Chem. Soc.* 120:7381–7382.

Lo, Y. L., and Y. E. Rahman. 1998. Effect of lipids on the thermal stability and conformational changes of proteins: ribonuclease A and cytochrome c. *Int. J. Pharm.* 161:137–148.

Morse, P. D., and D. W. Deamer. 1973. Interaction of cytochrome *c* with lipid monolayers. *Biochim. Biophys. Acta.* 298:769–782.

Muga, A., H. H. Mantsch, and W. K. Surewicz. 1991. Membrane binding induces destabilization of cytochrome *c* structure. *Biochemistry.* 30: 7219–7224.

Noinville, S., M. Revault, M. H. Baron, A. Tiss, S. Yapoudjian, M. Ivanova, and M. R. Verger. 2002. Conformational changes and orientation of *humicola lanuginosa* lipase on a solid hydrophobic surface: an in situ interface FTIR-ATR study. *Biophys. J.* 82:2709–2719.

Nuzzo, R. G., L. H. Dubois, and D. L. Allara. 1990. Fundamental studies of microscopic wetting on organic surfaces. 1. Formation and structural characterization of a self-consistent series of polyfunctional organic monolayers. *J. Am. Chem. Soc.* 112:558–569.

Oellerich, S., S. Lecomte, M. Paternostre, T. Heimburg, and P. Hildebrandt. 2004. Peripheral and integral binding of cytochrome c to phospholipid vesicles. *J. Phys. Chem. B.* 108:3871–3878.

Paquet, M.-J., M. Laviolette, M. Pezolet, and M. Auger. 2001. Two-dimensional infrared correlation spectroscopy study of the aggregation of cytochrome *c* in the presence of dimyristoylphosphatidylglycerol. *Biophys. J.* 81:305–312.

Pinheiro, T. J. T. 1994. The interaction of horse heart cytochrome *c* with phospholipid bilayers. Structural and dynamic effects. *Biochimie.* 76: 489–500.

Pinheiro, T. J. T., and A. Watt. 1994. Lipid specificity in the interaction of cytochrome *c* with anionic phospholipid bilayers revealed by solid-state $^{31}$P NMR. *Biochemistry.* 33:2451–2458.

Pott, T., M. Paternostre, and E. J. Dufourc. 1998. A comparative study of the action of melittin on sphingomyelin and phosphatidylcholine bilayers. *Eur. Biophys. J.* 27:237–245.

Quinn, P. J., and R. M. C. Dawson. 1969. The interaction of cytochrome c with monolayers of phosphatidylethanolamine. *Biochem. J.* 113: 791–803.

Rivas, L., D. H. Murgida, and P. Hildebrandt. 2002. Conformational and redox equilibria and dynamics of cytochrome c immobilized on electrodes via hydrophobic interactions. *J. Phys. Chem. B.* 106:4823–4830.

Salamon, Z., and G. Tollin. 1996a. Surface plasmon resonance studies of complex formation between cytochrome *c* and bovine cytochrome *c* oxidase incorporated into a supported planar lipid bilayer. I. Binding of cytochrome c to cardiolipin/phosphatidylcholine membranes in the absence of oxidase. *Biophys. J.* 71:848–857.

Salamon, Z., and G. Tollin. 1996b. Surface plasmon resonance studies of complex formation between cytochrome c and bovine cytochrome c oxidase incorporated into a supported planar lipid bilayer. II. Binding cytochrome c to oxidase-containing cardiolipin/phosphatidylcholine membranes. *Biophys. J.* 71:858–867.

Soulimane, T., G. Buse, G. P. Bourenkov, H. D. Bartunik, R. Huber, and M. E. Than. 2000. Structure and mechanism of the aberrant $ba_3$-cytochrome c oxidase from *Thermus thermophilus*. *EMBO. J.* 19:1766–1776.

Soulimane, T., M. Von Walter, P. Hof, M. E. Than, R. Huber, and G. Buse. 1997. Cytochrome $c_{552}$ from *Thermus thermophilus*: a functional and crystallographic investigation. *Biochim. Biophys. Res. Com.* 237:572–576.

Subramanian, M., A. Jutila, and K. J. Kinnunen. 1998. Binding and dissociation of cytochrome *c* to and from membranes containing acidic phospholipids. *Biochemistry.* 37:1394–1402.

Sukhishvili, S. A., and S. Granick. 1999. Adsorption of human serum albumin: dependence on molecular architecture of the oppositely charged surface. *J. Chem. Phys.* 110:10153–10161.

Surewicz, W. K., and H. H. Mantsch. 1988. New insight into protein secondary structure from resolution-enhanced infrared spectra. *Biochim. Biophys. Acta.* 952:115–130.

Than, M. E., P. Hof, R. Huber, G. P. Bourenkov, H. D. Bartunik, G. Buse, and T. Soulimane. 1997. *Thermus thermophilus* cytochrome $c_{552}$: a new highly thermostable cytochrome *c* structure obtained by MAD phasing. *J. Mol. Biol.* 271:629–644.

Wasserman, S. R., Y.-T. Tao, and G. M. Whitesides. 1989. Structure and reactivity of alkylsiloxane monolayers formed by reaction of alkyltrichlorosilanes on silicon substrates. *J. Am. Chem. Soc.* 5:1074–1087.

Zuckermann, M. J., and T. Heimburg. 2001. Insertion and pore formation driven by adsorption of proteins onto lipid bilayer membrane-water interfaces. *Biophys. J.* 81:2458–2472.